21st Australasian Fluid Mechanics Conference
Adelaide, Australia
10-13 December 2018

Coherent structures under different stratification stability conditions in the atmospheric surface layer

X.B. Li[1,2], N. Hutchins[1] , I. Marusic[1] and X.J. Zheng[3]

[1]Department of Mechanical Engineering
University of Melbourne, Parkville, Melbourne 3000, Australia

[2]Key Laboratory of Mechanics on Western Disaster and Environment
Lanzhou university, lanzhou 730000, China

[3]School of Mechano-Electronic Engineering
Xidian university, Xi'an 710071, China

Abstract

A field experiment was carried out on a dry flat bed of Qingtu Lake in Minqin, China to measure the velocity and temperature in the atmospheric surface layer (ASL) at high Reynolds number ($Re_\tau \sim O(10^6)$). The facility, the Qingtu Lake Observation Array (QLOA), permits synchronous multi-point measurements of three-dimensional wind velocity and temperature at different wall-normal and spanwise positions. Data were collected continuously during two three-month periods (March to May) over two years (2014 and 2015), from which 89 hours of high quality data were selected to analyse the characteristics of the large-scale coherent structures under different stratification stability conditions (strong unstable, weak unstable, near-neutral and stable conditions). In the unstable ASL, [1] indicate that the positive buoyancy essentially represents a wall-normal force, which likely has a "lifting" effect increasing the size of large-scale structures. By computing two-point correlations of the fluctuating streamwise velocity, this paper analyses such effects using this unprecedented dataset collected under different stratification stability conditions. The results confirm the previous findings and further illustrate that negative buoyancy in the stable condition has an opposite effect leading to small structures with less wall-normal coherence. The unique measurement array at this facility also permits us to study the three-dimensional form of these features, and the associated temperature fluctuations which are also discussed in this work.

Introduction

Experimental and numerical studies identified that various types of coherent structures exist within the turbulent boundary layer (see the review by Robinson [8]). The vast majority of laboratory studies of boundary-layer turbulence have been conducted at low to moderate Reynolds numbers [$Re_\tau = O(10^3 - 10^4)$] and in neutral conditions. As mentioned by Guala *et al.* [3], the near-neutral ASL can be seen as a true high-Reynolds-number facility ($Re_\tau = \delta u_\tau/\nu = O(10^6)$, where δ is the atmospheric surface-layer thickness, u_τ is the skin-friction velocity and ν is the kinematic viscosity). Hutchins *et al.* [5] revealed remarkable similarity for the first time when comparing the coherent structure features observed in the near-neutral ASL with low Reynolds number laboratory data. Carper and Porté-Agel [1] found that the structure inclination angle is a strong function of atmospheric stability, varying between 15° and 35°. Recently, Chauhan *et al.* [2] also demonstrated that the inclination angle changes drastically under different stability conditions, varying systematically with the Monin–Obukhov stability parameter in the unstable regime.

In this study, two-point correlations of the fluctuating velocity and teperature are examined in the atmospheric surface layer.

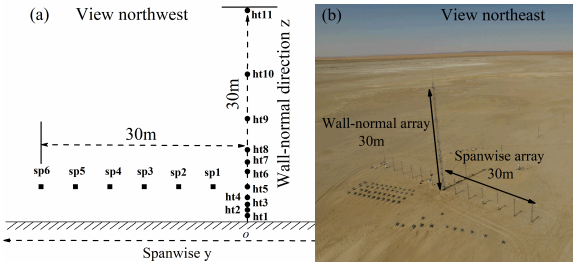

Figure 1: (a) Northwest view of the sonic anemometer array, the solid squares labelled spi (i=1, 2, ..., 6) and the solid circles htj (j=1, 2, ..., 11) represent the spanwise and wall-normal anemometer array respectively. (b) Northeast view of the measurement array installed at the QLOA.

The two-point correlation of the streamwise velocity component u is defined as:

$$R_{uu}(\Delta x, \Delta y, \Delta z) = \frac{< u(x,y,z)u(x+\Delta x, y+\Delta y, z+\Delta z) >}{\sigma_{u(x,y,z)}\sigma_{u(x+\Delta x, y+\Delta y, z+\Delta z)}} \quad (1)$$

where Δx is converted from the temporal lead/lag using Taylor's hypothesis of frozen turbulence ($\Delta x = U\Delta t$, U is the convection velocity taken as the mean velocity at the corresponding wall-normal position z), Δy and Δz are the relative width and height from the reference point, and the angle bracket "<>" indicates long time averages. Based on the high Reynolds number ASL experimental data, the purpose of the present effort is to explore the coherent structures under different kinds of stability conditions by the two-point correlations.

Experimental Facility

A field experiment was carried out on a dry flat bed of Qingtu Lake in Minqin, China to measure the three-dimensional velocity and temperature in streamwise, spanwise and wall-normal directions in the ASL at high Reynolds number($Re_\tau \sim O(10^6)$). The QLOA site is located on a sand surface between the Badain Jaran Desert and the Tenger Desert (N39°12.17′ E103°40.03′). The three components of wind velocity and the temperature were acquired by sonic anemometers (Gill Instruments R3-50) with a sampling rate of 50 Hz (all seventeen anemometers are sampled simultaneously). Figure 1 shows the anemometer array and an overview of the QLOA site. The seventeen anemometers (used in this work) were installed at the main tower and six spanwise lower towers. The main tower is 32 m high and the remaining lower towers are 5 m in height. The span-wise array covered an overall distance of 30m with 7 anemometers placed 5m apart and at the height of $z = 5$m. The wall-normal

Wall_normal array	y (m)	z (m)	Spanwise array	y (m)	z (m)
ht1	0	0.9	ht5	0	5
ht2	0	1.71	sp1	5	5
ht3	0	2.5	sp2	10	5
ht4	0	3.49	sp3	15	5
ht5	0	5	sp4	20	5
ht6	0	7.15	sp5	25	5
ht7	0	8.5	sp6	30	5
ht8	0	10.24			
ht9	0	14.65			
ht10	0	20.96			
ht11	0	30			

Table 1: $y-z$ coordinates of the 17 annemometers.

array consisted of 11 sonic anemometers installed with a logarithmic spacing from $z = 0.9$ to 30m, and 11 anemometers were installed in a logarithmic manner ($z =$ 0.9, 1.71, 2.5, 3.49, 5, 7.15, 8.5, 10.24, 14.65, 20.96, 30m). The spanwise and wall-normal coordinates for each of the 17 anemometers are given in Table 1. It should be noted that the first sonic anemometer in the spanwise array is shared with the fifth on the main tower, which means we have 7 available anemometers in the spanwise array. Data were collected continuously during two three-month periods (March to May) over two years (2014 and 2015). A total of 89 hours (from a total of more than 3000 hours collected) of high quality data were selected after a series of pretreatment operations described below.

Data Selection

For observations in the atmospheric surface layer, much of the acquired data are unsuitable for this type of analysis owing to variable or unsuitable prevailing conditions. The usable data were selected by following similar methods to those outlined in Hutchins *et al.* [5] where we seek periods of relatively steady conditions, where the wind is coming from an appropriate direction, and where the mean direction is relatively constant. Wind direction adjustment, de-trending manipulation, steady wind selection and stability judgement are introduced in details in Wang and Zheng [10]. The friction velocity u_τ is obtained from $u_\tau = (-\overline{uw})^{1/2}$ at $z = 5$ m (calculated by ht5). The thermal stability of the ASL is generally characterized by the Monin-Obukhov stability parameter z/ζ, which is defined as

$$\frac{z}{\zeta} = -\frac{\kappa z g \overline{w\theta}}{\overline{\theta} u_\tau^3} \tag{2}$$

and where $\kappa = 0.41$ is the kármán constant, g is the gravitational acceleration, $\overline{w\theta}$ is the surface heat flux, and $\overline{\theta}$ is the mean temperature. We assume an estimate for the surface-layer thickness of $\delta = 60$ (same as Hutchins *et al.* [5]). The 89 hours of data remaining after preselection are divided into 4 datasets based on the value of the stratification stability parameter. Part 1 contains periods with the a stability parameter $z/\zeta < -0.3$, which indicates the strong unstable condition. Part 2 contains periods which exhibit a weaker unstable behaviour within the range $-0.3 \leq z/\zeta < -0.03$. Part 3 represents the near-neutral condition defined here as $-0.03 \leq z/\zeta < 0.03$. The final part (4) represents the stable condition data $z/\zeta \geq 0.03$. The percentage occurrence for parts 1 - 4 are 22.5%, 55.1%, 11.2% and 11.2%, respectively.

In the absence of a direct measure for the boundary layer thickness, we have to assume a certain value of δ for consistency across a range of measured statistics. [6] and [5] seemed to choose 60 m as the proper boundary layer thickness δ to compare well with laboratory data in statistics and the two-point correlation results. [10] and [7] estimated the boundary layer thickness δ based on the formulation of the streamwise turbulent intensity. However, [9] and [4] point out that the boundary layer thickness δ varies significantly between the stable and unstable conditons. The value of δ depends strongly on the convection intensity and direction. This poses a real challenge for studies such as this, where we wish to detrend data, and analyse the dominant coherent structure under different stability conditions. As mentioned in [5], correlation estimates can be extremely sensitive to long-term (non-turbulence related) trends in the data. Results of [6] suggest that events of length $10\delta-20\delta$ are not uncommon in laboratory-scale turbulent boundary layers. Since the filter scales used to seperate turbulence from weather related phenomena are usually scaled in terms of δ, the lack of a reliable estimate here is problematic. For future measurements, an independent measure of δ via LIDAR measurements would greatly assist in this endeavour. An additional sonic placed a greater distance away from the main array (at least several hundred meters) would also greatly assist in detrending. Any energy that was coherent between this remote measurement and the main array could be considered as non-turbulent information to be filtered out in the detrending procedure. In the absence here of this information a constant $\delta = 60$ m is assumed throughout this analysis in line with [5].

Results

Throughout this paper u, v, w and θ refer to the fluctuating velocities in the streamwise (x), spanwise (y), and wall-normal (z) directions and the temperature component, respectively.

Two-point correlation

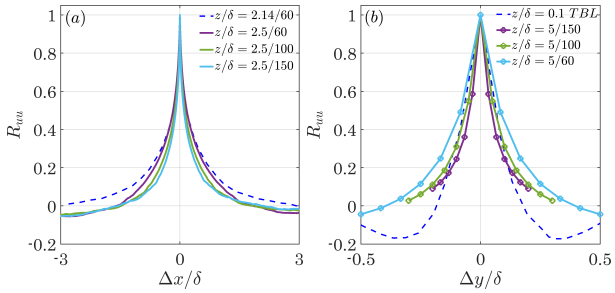

Figure 2: Two-point correlations of the streamwise velocity fluctuation R_{uu} calculated for the near-neutral ASL data in (a) streamwise, and (b) spanwise direction. Dash blue line in (a) shows the ASL result from [6], at comparable $z/\delta = 2.14/60$ and in (b) shows the TBL result what about the ASL result from [5] ([6], $z/\delta = 0.1$).

Figure 2 (a) shows the auto-correlations in the streamwise direction for $z/\delta \approx 2.5/60$ compared with the ASL and laboratory TBL results in [6]. It should be noted that we have here used the same preprocessing methods as [6] to obtain the turbulence related signals. In general, the current ASL data in Figure 2 (a) matches well the results in literature for the range $-1 < \Delta x/\delta < 1$, however, beyond this range differences are observed. Though there are many factors that may explain these differences (difference in terrain, humidity etc), we feel that the most likely culprit will be the preprocessing, and in particular the detrending operation. The data are filtered at a length $\lambda_x = 15\delta$. The additional curves on figure 2 (a) show the same data with a different assumed delta of 100m and 150m. Figure 2 (b) shows the two-point correlation across the spanwise array. This time the difference between the current ASL data, and results in the literature are more pronounced. Though there is rea-

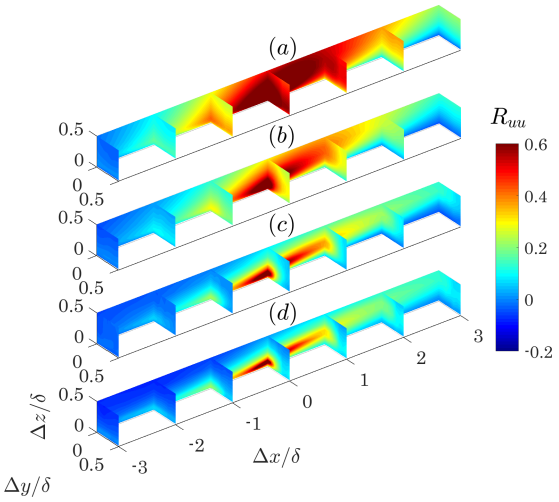

Figure 3: Iso-contours of R_{uu}. Contour levels for all plots are from R_{uu} = -0.2 to 0.6.

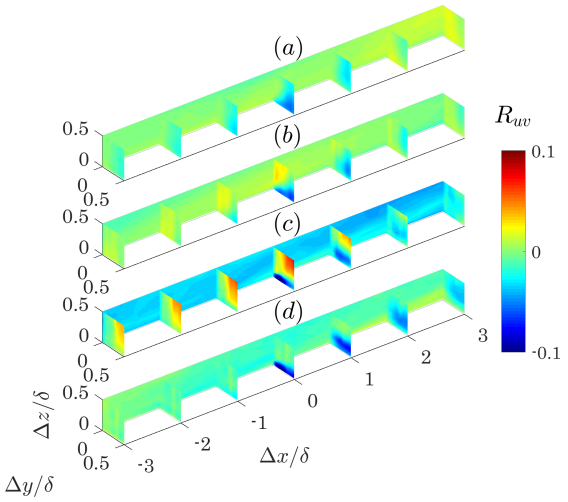

Figure 4: Two-point cross-correlations of streamwise velocity fluctuation with spanwise velocity fluctuation R_{uv}. Contour levels for all plots are from R_{uv} = -0.1 to 0.1.

sonable collapse for $-0.1 < \Delta y/\delta < 0.1$, the negative lobes that have typically been observed in such studies are no-longer visible. Again the additional curves on this plot which show results when we assume $\delta = 100$m and $\delta = 150$m, give some indication of the sensitivity to the assumed boundary layer thickness and to the filter scale.

A 3D view of the large-scale coherence

In this section, we build up a three-dimensional view of the large-scale coherence using the correlations R_{uu}, R_{uv}, R_{uw} and $R_{u\theta}$ under four different stratification stability conditions. By varying the reference point location for the two-point correlations to different anemometers along the spanwise array, it is possible to produce a volumetric correlation map. For convenience of comparasion, (a), (b), (c) and (d) for the following plots all represent the strong unstable, weak unstable, near-neutral and stable stratification stability conditions, respectively. All plots depict a three-dimensional view of the $x-z$ plane at $\Delta y = 0$ and seven equi-spaced $y-z$ planes at $\Delta x/\delta = -3,-2,-1,0,1,2,3$. These planes are chosen for clarity and to illustrate key features of the correlation maps.

Figure 3 shows the two-point correlation of the streamwise veloccty component R_{uu}. For all stability conditions, a highly elongated region of positive correlation at the reference position is apparent. The region of positive correlation shows that the coherent structure has a large wall-normal extent and is extremely persistent in the streamwise direction. It appears that the unstable surface layer has a larger spatial extent of meaningful correlation and hence the underlying coherence occurs at a larger physical scale, which is opposite to the stable condition. Buoyancy in the atmospheric surface layer essentially represents a force that acts normal to the preferred orientation of these structures. Thus, positive buoyancy can be interpreted to have a 'lifting' effect, with a "suppressing" occurring effect under the action of negative buoyancy in the stable condition.

Figures 4 to 6 explore the correlations of u fluctuations with the remaining two velocity components and scalar temperature. Figure 4 shows the correlation between the streamwise and spanwise velocity fluctuations (R_{uv}) . At $\Delta x/\delta = 0$ and $\Delta y/\delta > 0$, all four conditions exhibit an arrangement of anti-correlated behavior close to the wall giving way to a region of positive correlation further from the wall. The two point correlations are unsigned, but if we consider a negative u fluctuation at the origin (which is essentially forming a Linear Stochastic Estimate), this will be accompanied by spanwise converging flow close to the wall, giving way to spanwise diverging flow at greater values of z. This pattern is typically the tell-tale sign of counter-rotating roll-modes accompanying the elongated low and high momentum regions. It is evident that in the unstable condition (figure 4a) the wall-normal extent of the anti-correlation is larger, indicating larger (diameter) roll-modes. Since these roll-modes are known to be inclined to the wall, this may also be a reflection of a steeper inlination angle of these roll-modes under unstable conditions. Under stable conditions (figure 4d), the opposite situation occurs, the regions of negative and positive correlation in R_{uv} are surpressed to a much smaller wall-normal extent, opposite to the stable condition.

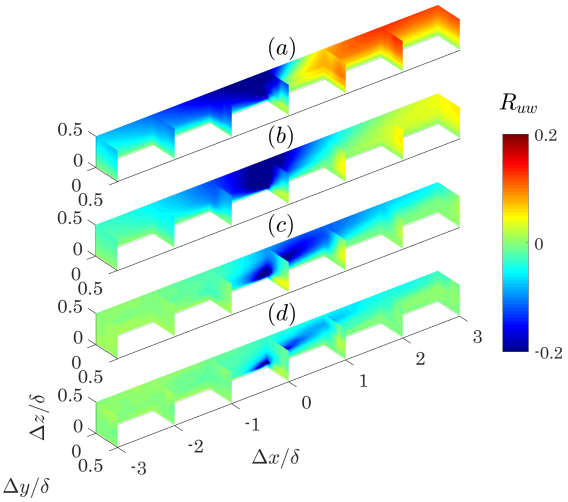

Figure 5: Two-point cross-correlations of streamwise velocity fluctuation with wall-normal velocity fluctuation R_{uw}. Contour levels for all plots are from R_{uw} = -0.2 to 0.2.

The corresponding streamwise–wall-normal correlation (R_{uw}) contours are shown in Figure 5. The R_{uw} correlation exhibits a notable asymmetry in the streamwise direction, such that in the near-neutral and stable conditions the correlation has a longer tail for positive Δx than for negative Δx. For the unstable conditions (figure 5a and 5b) the opposite is true, with the R_{uw} contours seeming to exhibit a backwards inclination. The anti-correlations on the reference plane (at $\Delta y/\delta = 0$) are flanked in

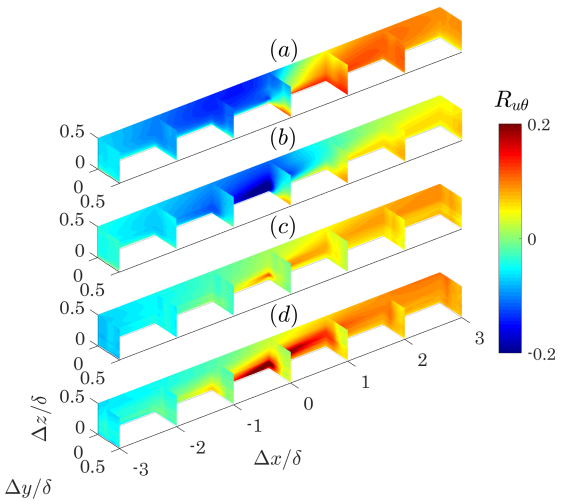

Figure 6: Two-point cross-correlations of streamwise velocity fluctuation with temperature fluctuation $R_{u\theta}$. Contour levels for all plots are from $R_{u\theta}$ = -0.1 to 0.1.

the spanwise direction by regions of positive correlation. This suggest that a low momentum event at the reference point will be accompanied by flow away from wall, with flow towards the wall occurring some distance away to the span. This again is consistent with the notion of counter-rotating roll-modes accompanying these events. There are signs that such roll-modes will be larger for the unstable cases, with a steeper inclination, while for the stable case they are more constrained to the wall.

The correlations of u fluctuations with the associated temperature fluctuations are shown in figure 6. It is obvious that the stable condition and the unstable condition have the opposite correlation around the reference point with the unstable region indicating a strong anti-correlation as expected, and the stable case exhibiting strong positive correlation. This is expected since u is anticorrelated with w at the reference point (see figure 5), and for the stable case w would be positively correlated with θ (where the wall-normal temperature gradient is positive), while this correlation between w and θ would be negative in the unstable case. However, the shape of the $R_{u\theta}$ contours are markedly different to those of R_{uw}, which deserves further investigation. The negatively correlated region for the unstable cases is strongly skewed in the upstream direction, while the positively correlated region for the stable case is skewed in the downstream. In addition, we would expect the near-neutral case to exhibit near zero correlation for $R_{u\theta}$. The fact that this is not the case, suggests that in future a much tighter constraint on this condition may be required. At present the near-neutral case exhibits a $R_{u\theta}$ behaviour that would be associated with a weakly stable condition.

Conclusions

The three-dimensional correlation of u events is analysed to reveal the underlying average large-scale structure under unstable, near-neutral and stable conditions. Significant differences in all correlations analysed (R_{uu}, R_{uv}, R_{uw} and $R_{u\theta}$) are observed between the different stability conditions. In general, the unstable cases produce extend regions of coherence, that are significantly longer and wider than the other cases. The wall-normal fluctuations w associated with the large-scale u events in these cases appear to be noticeably tilted backwards (upstream), which is in stark contrast to the near-neutral case, suggesting a substantially modified structure. The stable case seems to exhibit a similar structure to the near-neutral, albeit one with a smaller coherence, and that is prevented from growing so far from the wall. The results of the present work contribute to a better understanding of the coherent structures under the unstable, near-neutral and stable stratification stability conditions. In the future, the vortical structures associated with these events will be studied in more detail, and asymmetries between positive and negative u events will be explored using conditional averaging.

Acknowledgements

NH and IM acknowledge support from the Australian Research Council. XJZ and XBL acknowledge support from the Naitonal Natural Science Foundation of China. XBL is also supported by CSC scholarship (File No. 201706180037) .

References

[1] Carper, M. A. and Porté-Agel, F., The role of coherent structures in subfilter-scale dissipation of turbulence measured in the atmospheric surface layer, *J. Turbul.*, **5**, 2004, 32–32.

[2] Chauhan, K., Hutchins, N., Monty, J. and Marusic, I., Structure inclination angles in the convective atmospheric surface layer, *Bound.-Lay. Meteorol.*, **147**, 2013, 41–50.

[3] Guala, M., Metzger, M. and McKeon, B., Interactions within the turbulent boundary layer at high reynolds number, *J. Fluid Mech.*, **666**, 2011, 573–604.

[4] Huang, M., Gao, Z., Miao, S., Chen, F., LeMone, M. A., Li, J., Hu, F. and Wang, L., Estimate of boundary-layer depth over beijing, china, using doppler lidar data during surf-2015, *Bound.-Lay. Meteorol.*, **162**, 2017, 503–522.

[5] Hutchins, N., Chauhan, K., Marusic, I., Monty, J. and Klewicki, J., Towards reconciling the large-scale structure of turbulent boundary layers in the atmosphere and laboratory, *Bound.-Lay. Meteorol.*, **145**, 2012, 273–306.

[6] Hutchins, N. and Marusic, I., Evidence of very long meandering features in the logarithmic region of turbulent boundary layers, *J. Fluid Mech.*, **579**, 2007, 1–28.

[7] Liu, H., Wang, G. and Zheng, X., Spatial length scales of large-scale structures in atmospheric surface layers, *Physical Review Fluids.*, **2**, 2017, 064606.

[8] Robinson, S. K., Coherent motions in the turbulent boundary layer, *Annu. Rev. Fluid Mech.*, **23**, 1991, 601–639.

[9] Svensson, G., Holtslag, A., Kumar, V., Mauritsen, T., Steeneveld, G., Angevine, W., Bazile, E., Beljaars, A., De Bruijn, E., Cheng, A. et al., Evaluation of the diurnal cycle in the atmospheric boundary layer over land as represented by a variety of single-column models: the second gabls experiment, *Bound.-Lay. Meteorol.*, **140**, 2011, 177–206.

[10] Wang, G. and Zheng, X., Very large scale motions in the atmospheric surface layer: a field investigation, *J. Fluid Mech.*, **802**, 2016, 464–489.